

β -decay rates of neutron-rich Zr and Mo isotopes in the deformed quasiparticle random-phase approximation with realistic interactions

Dongdong Ni^{1,2,*} and Zhongzhou Ren^{1,2,3,4,†}¹*Department of Physics and Key Laboratory of Modern Acoustics, Institute of Acoustics, Nanjing University, Nanjing 210093, China*²*Joint Center of Nuclear Science and Technology, Nanjing University, Nanjing 210093, China*³*Kavli Institute for Theoretical Physics China, Beijing 100190, China*⁴*Center of Theoretical Nuclear Physics, National Laboratory of Heavy-Ion Accelerator, Lanzhou 730000, China*

(Received 8 May 2014; revised manuscript received 10 June 2014; published 30 June 2014)

The β^- -decay rates of neutron-rich Zr and Mo isotopes are investigated within the deformed quasiparticle random-phase approximation with realistic nucleon-nucleon interactions. Axially symmetric deformations are considered in the calculations from a mean-field description of a quasiparticle picture and of both particle-hole and particle-particle excitations. The Brückner G matrix obtained with charge-dependent Bonn nucleon-nucleon forces is employed for residual particle-particle and particle-hole interactions. Contributions from both allowed Gamow-Teller and first-forbidden transitions are calculated and the sensitivity of the calculated results to the particle-particle strength is discussed. The calculated β -decay half-lives show a good agreement with the available experimental data. Moreover, predictions of β -decay half-lives are made for some extremely neutron-rich isotopes, which could be useful for future experiments.

DOI: [10.1103/PhysRevC.89.064320](https://doi.org/10.1103/PhysRevC.89.064320)

PACS number(s): 23.40.-s, 21.10.Tg, 21.30.Fe, 21.60.Jz

I. INTRODUCTION

Over the last decade, considerable attention has been paid to both experimental and theoretical investigations of neutron-rich Zr and Mo isotopes due to their importance in understanding nuclear structure and astrophysics. From the viewpoint of nuclear structure, the available experimental studies on structural evolution [1,2] have shown that the quadrupole deformation reaches a maximum at $N = 64$ and gradually decreases with increasing neutron number up to $N = 68$ for Zr and Mo isotopes, confirming the existence of the deformed subshell closure $N = 64$. But the evolution of the deformation beyond $N = 68$ is still unknown because experimental spectroscopic measurements at the present facilities are unavailable. Theoretically, predictions of shape transitions are made for more exotic isotopes with $N \geq 70$, such as the finite-range droplet model (FRDM) [3], deformed Woods-Saxon model [4], relativistic mean-field (RMF) model [5], Hartree-Fock plus BCS method [6], and Hartree-Fock-Bogoliubov model [7].

From the viewpoint of nuclear astrophysics, very neutron-rich Zr and Mo isotopes are involved in the rapid neutron-capture process (r process), which proceeds through a chain of very neutron-rich nuclei and creates approximately half of the nuclei heavier than iron in nature. Their β -decay information is required to determine not only the nuclear r -process time scale but also the abundances of elements [8–10]. Consequently, efforts have been devoted to measure β -decay properties of very neutron-rich Zr and Mo isotopes. Some new data have been measured with improved accuracy and some have even been observed for the first time [11,12]. Very impressively, the β -decay half-lives of 38 neutron-rich

isotopes in the $A \approx 100$ region have been measured at RIKEN, suggesting a more rapid matter flow of the r process through this region than previously predicted [12]. In spite of these achievements, experimental measurements for more exotic nuclei near the neutron drip line are still unavailable at present. For these exotic nuclei, one has to resort to reliable theoretical predictions. As neutron-rich Zr and Mo isotopes are generally deformed, and furthermore, β -decay rates of neutron-rich nuclei as well as matrix elements of double β decay are affected by nuclear deformations [13,14], it is of utmost importance for theoretical calculations to take the deformations into account. Several deformed calculations based on the quasiparticle random-phase approximation (QRPA) have been established. For example, there are deformed QRPA calculations with schematic separable Gamow-Teller (GT) forces, where different ground-state descriptions are employed such as the FRDM plus folded-Yukawa single-particle (s.p.) potential [10], deformed Woods-Saxon potential [13,14], deformed Nilsson s.p. levels [15], and deformed Skyrme-Hartree-Fock (SHF) calculations [13,16]. Based on the deformed SHF model, the deformed QRPA with consistent residual interactions was developed for GT strengths in Ref. [17]. The authors of Ref. [18] developed the self-consistent deformed QRPA with finite-range Gogny interactions on top of deformed Hartree-Fock-Bogoliubov calculations. Also, the deformed QRPA with realistic nucleon-nucleon interactions has been developed for both two-neutrino and neutrinoless double β decays [19,20], and it has been extended to investigate β decay [21].

All these efforts by and interest from both the experimental and the theoretical sides encourage us to take into account the deformations and investigate the β -decay rates of neutron-rich Zr and Mo isotopes. Recently, we have investigated β^- decays of r -process waiting-point nuclei around the neutron magic numbers within the extended QRPA with neutron-proton pairing [22]. Within this model, two-body interaction matrices are obtained with realistic nucleon-nucleon interactions and

*dongdongnick@gmail.com.

†zren@nju.edu.cn.

calculations are performed on the spherical s.p. basis. As a further improvement, the present study reports on the deformed QRPA with realistic nucleon-nucleon interactions constructed on the deformed s.p. basis. Progress has been made in two ways: On the one hand, nuclear deformations are taken into account, following the path from a deformed s.p. description, to a deformed quasiparticle picture, and to deformed QRPA calculations. On the other hand, first-forbidden (FF) transitions are considered in the response functions, besides allowed GT transitions. Numerically, good stability is required for program codes and computation time increases greatly when nuclear deformations are considered. The reasons for this are that the highly degenerate spherical s.p. basis is transformed into the doubly degenerate deformed s.p. basis, leading to an obvious increase in the dimension of QRPA matrix equations, and it is not the total angular momentum but the projection of the total angular momentum on the symmetric axis that serves as a good quantum number. Efforts have been made from the theoretical and numerical sides.

This article is organized in the following way. Section II briefly shows the key points of β -decay calculations and the framework of the deformed QRPA. In Sec. III, the dependence of our calculations on model parameters is discussed in detail, and the theoretical results of our calculations are compared with the experimental data and other theoretical results. A summary is given in Sec. IV.

II. THEORETICAL FRAMEWORK

The process of β decay generally occurs from an initial ground state i in a parent nucleus to some final states in the daughter nucleus. The partial half-life t for a β^- transition $i \rightarrow f$ is obtained using the expression $f(Z, R, W_0) \times t = 6170$ s, with [23,24]

$$f(Z, R, W_0) = \int_1^{W_0} dW C(W) F(Z, R, W) (W_0 - W)^2 \times W \sqrt{W^2 - 1}. \quad (1)$$

In Eq. (1), W_0 and W are the maximum energy and the total energy (including the rest energy) of the β particle; Z and R are separately the atomic number and the nuclear radius of the daughter nucleus; $C(W)$ is the so-called shape factor, which describes the reduced transition probability; and $F(Z, R, W)$ is the Fermi function, which accounts for the Coulomb interaction between the charged β particle and the residual daughter nucleus [25,26]. Note that expression (1) is written in natural units ($\hbar = m_e = c = 1$) so that the units of energy and length are given by $m_e c^2$ and $\hbar/m_e c$, respectively. The β maximum energy W_0 for β^- decay is given by $W_0 = (Q_\beta - E_{\text{ex}})/m_e c^2 + 1$, where E_{ex} is the excitation energy of the final state with respect to the ground state of the daughter nucleus. The occurrence of β^- decay requires $W_0 > 1$. That is, the final states of β^- transitions have to exhibit the excitation energies $E_{\text{ex}} < Q_\beta$. Hence, the β -decay half-life is calculated by summing all allowed f values for GT and FF transitions,

$$T_{1/2} = \frac{6170 \text{ s}}{\sum_{E_{\text{ex}} < Q_\beta} [f_{\text{GT}}(Z, R, E_{\text{ex}}) + f_{\text{FF}}(Z, R, E_{\text{ex}})]}. \quad (2)$$

For GT transitions, the shape factor is not dependent on the β energy W and has the form [27–34]

$$C(W) = B(GT) = \left(\frac{g_A}{g_V}\right)^2 \frac{1}{2J_i + 1} |\langle f \| \vec{\sigma} \vec{\tau}_+ \| i \rangle|^2, \quad (3)$$

where $\vec{\tau}_+$ is the isospin raising operator, $\vec{\tau}_+ |n\rangle = |p\rangle$, and $\vec{\sigma}$ is the Pauli spin matrix.

In the case of FF transitions, the shape factor depends on the β energy W . If only dominant terms are considered, it can be written as

$$C(W) = k(1 + aW + b/W + cW^2). \quad (4)$$

According to the treatment by Behrens and Bühring [25,26], the detailed expressions of k , ka , kb , and kc are

$$k = \left[\zeta_0^2 + \frac{1}{9}\omega^2\right] + \left[\zeta_1^2 + \frac{1}{9}(x+u)^2 - \frac{4}{9}\mu_1\gamma_1 u(x+u) + \frac{1}{18}W_0^2(2x+u)^2 - \frac{1}{18}\lambda_2(2x-u)^2\right] + \frac{1}{12}z^2(W_0^2 - \lambda_2), \quad (5a)$$

$$ka = -\frac{4}{3}uY - \frac{1}{9}W_0(4x^2 + 5u^2) - \frac{1}{6}z^2W_0, \quad (5b)$$

$$kb = \frac{2}{3}\mu_1\gamma_1[-\zeta_0\omega + \zeta_1(x+u)], \quad (5c)$$

$$kc = \frac{1}{18}[8u^2 + (2x+u)^2 + \lambda_2(2x-u)^2] + \frac{1}{12}z^2(1 + \lambda_2), \quad (5d)$$

with

$$\begin{aligned} \gamma_1 &= \sqrt{1 - (\alpha Z)^2}, \quad V = \xi'v + \xi w', \quad \zeta_0 = V + \omega W_0/3, \\ Y &= \xi'y - \xi(u' + x'), \quad \zeta_1 = Y + (u - x)W_0/3, \end{aligned} \quad (6)$$

where $\xi = \alpha Z/2R$, α is the fine-structure constant and R is the radius of a uniformly charged sphere approximating the nuclear charge distribution. The quantities μ_1 and λ_2 are associated with electron wave functions and momentum [25,26]. Their values are approximated as $\mu_1 \approx 1$ and $\lambda_2 \approx 1$ [24]. The nuclear matrix elements can be expressed in terms of form-factor coefficients ${}^{A,V}F_{K\ell s}$ defined by Behrens and Bühring [25,26]. In the Biedenharn-Rose phase convention, the nonrelativistic matrix elements are given by [23,35]

$$\omega = -R^A F_{011}^0 = -\eta\sqrt{3}\langle f \| ir[\mathbf{C}_1 \times \vec{\sigma}]^0 \vec{\tau}_+ \| i \rangle C, \quad (7a)$$

$$x = -R^V F_{110}^0/\sqrt{3} = -\langle f \| ir\mathbf{C}_1 \vec{\tau}_+ \| i \rangle C, \quad (7b)$$

$$u = -\sqrt{2/3}R^A F_{111}^0 = -\eta\sqrt{2}\langle f \| ir[\mathbf{C}_1 \times \vec{\sigma}]^1 \vec{\tau}_+ \| i \rangle C, \quad (7c)$$

$$z = \sqrt{4/3}R^A F_{211}^0 = \eta 2\langle f \| ir[\mathbf{C}_1 \times \vec{\sigma}]^2 \vec{\tau}_+ \| i \rangle C, \quad (7d)$$

$$\xi'v = {}^A F_{000}^0 = \eta\sqrt{3}\langle f \| \frac{i}{M}[\vec{\sigma} \times \vec{\nabla}]^0 \vec{\tau}_+ \| i \rangle C, \quad (7e)$$

$$\xi'y = {}^V F_{101}^0 = -\langle f \| \frac{i}{M}\vec{\nabla} \vec{\tau}_+ \| i \rangle C, \quad (7f)$$

where $\eta = g_A/g_V$, $C = 1/\sqrt{2J_i + 1}$, and $\mathbf{C}_{\ell m} = \sqrt{4\pi/(2\ell + 1)}\mathbf{Y}_{\ell m}$, and M is the nucleon mass. The matrix elements ω' , x' , and u' take into account the nuclear charge distribution. They can be obtained from the definitions of ω , x , and u by including in the radial integral an extra

factor [26]:

$$I(1,1,1,1,r) = 3/2[1 - (r/R)^2/5], \quad 0 \leq r \leq R, \\ = 3/2[R/r - (R/r)^3/5], \quad r \geq R. \quad (8)$$

In order to evaluate the nuclear matrix elements, we need to know the wave functions of the initial and final nuclear states, $|i\rangle$ and $|f\rangle$. Here, they are calculated within the deformed QRPA with realistic nucleon-nucleon interactions. The picture we consider here is that of an axially symmetric deformed system with the set of deformation parameters $(\beta_2, \beta_4, \beta_6)$. It is convenient to use an intrinsic coordinate frame to describe such a system [36,37]. In this frame, the projection K of the angular momentum on the symmetric axis and the parity π are good quantum numbers. So one can separately perform both mean-field and QRPA calculations in each K^π block. The intrinsic excitations are defined by QRPA phonon excitation operators [27–33],

$$Q_{m,K^\pi}^\dagger = \sum_{pn} [X_{pn,K^\pi}^m \alpha_p^\dagger \alpha_n^\dagger - Y_{pn,K^\pi}^m a_{\bar{p}} a_n], \quad (9)$$

where X_{pn,K^π}^m and Y_{pn,K^π}^m are, respectively, the forward- and backward-going amplitudes of the m th QRPA phonon characterized by K^π , α_τ^\dagger (α_τ) are quasiparticle creation (annihilation) operators, $\tau = p, n$ denotes the proton and neutron quasiparticle states, and α_τ^\dagger (α_τ) are the time-reversed operators of α_τ^\dagger (α_τ). The sum runs over the quasiparticle pairs $p\bar{n}$ which satisfy the rules $\Omega_p - \Omega_n = K$ and $\pi_p \pi_n = \pi$, where Ω_τ is the projection of the total angular momentum on the nuclear symmetric axis and π_τ is the parity. The QRPA excited states $|mK^\pi\rangle$ are generated by the QRPA phonon excitation operator acting on the QRPA ground state $|\tilde{0}\rangle$, i.e., $|mK^\pi\rangle = Q_{m,K^\pi}^\dagger |\tilde{0}\rangle$. The usual QRPA matrix equations have the form [27–33]

$$\begin{pmatrix} A(K^\pi) & B(K^\pi) \\ -B(K^\pi) & -A(K^\pi) \end{pmatrix} \begin{pmatrix} X_{K^\pi}^m \\ Y_{K^\pi}^m \end{pmatrix} = \omega_{K^\pi}^m \begin{pmatrix} X_{K^\pi}^m \\ Y_{K^\pi}^m \end{pmatrix}, \quad (10)$$

where $\omega_{K^\pi}^m$ are the energy eigenvalues characterizing the energies of the m th QRPA phonon state. The submatrices A and B are given by

$$A_{pn,p'n'}(K^\pi) = (E_p + E_n) \delta_{pn,p'n'} \\ + g_{pp}(u_p u_n u_{p'} u_{n'} + v_p v_n v_{p'} v_{n'}) V(p\bar{n} p' \bar{n}') \\ + g_{ph}(u_p v_n u_{p'} v_{n'} + v_p u_n v_{p'} u_{n'}) \tilde{V}(pn' p'n), \quad (11)$$

$$B_{pn,p'n'}(K^\pi) = -g_{pp}(u_p u_n v_{p'} v_{n'} + v_p v_n u_{p'} u_{n'}) V(p\bar{n} p' \bar{n}') \\ + g_{ph}(u_p v_n v_{p'} u_{n'} + v_p u_n u_{p'} v_{n'}) \tilde{V}(pn' p'n), \quad (12)$$

where E_p and E_n are, respectively, the proton and neutron quasiparticle energies; v and u are, respectively, the occupation and unoccupation amplitudes for one s.p. state, $v^2 + u^2 = 1$; and \tilde{V} and V separately denote the particle-hole (ph) and particle-particle (pp) interaction matrices of the residual proton-neutron interaction. The amplitude for β^- transitions from the ground state $|\tilde{0}\rangle$ of an even-even nucleus to the m th phonon state $|mK^\pi\rangle$ of the neighboring odd-odd nucleus is

expressed in the intrinsic frame by [19,20]

$$\beta^- \equiv \langle mK^\pi | \beta_{JK}^- | \tilde{0} \rangle \\ = \sum_{pn} \langle p | T_{JK} | n \rangle [u_p v_n X_{pn,K}^m + v_p u_n Y_{pn,K}^m], \quad (13)$$

where the operators T_{JK} denote the GT transition operator, Eq. (3), and the FF transition operators, Eq. (7). To obtain the transition amplitude in the laboratory frame, one needs to express the initial and final states in the laboratory frame in terms of the intrinsic states and employ the transformation of the operators. The details for the transformation from the intrinsic frame to the laboratory frame can be found in Refs. [36] and [37]. Besides, in the case of an even-even nucleus, the excitation energy E_{ex} of the final state can be simply obtained by subtracting a reference energy E_0 from the QRPA energy $\omega_{K^\pi}^m$, i.e., $E_{\text{ex}} = \omega_{K^\pi}^m - E_0$, where E_0 is the lowest two-quasiparticle energy associated with the ground state of the odd-odd daughter nucleus [16,18,22].

The deformed s.p. states $|p\rangle$ and $|n\rangle$ are computed by solving the Schrödinger equation in an axially deformed Woods-Saxon potential [38]. The deformed s.p. wave functions $|\tau\Omega_\tau\rangle$ are decomposed as [19,20]

$$|\tau\Omega_\tau\rangle = \sum_{Nn_z\Sigma} b_{Nn_z\Sigma} |Nn_z\Lambda = \Omega_\tau - \Sigma\rangle |\Sigma\rangle, \quad (14)$$

where $|Nn_z\Lambda\rangle$ is the deformed harmonic oscillator s.p. wave function with the principal quantum numbers $(Nn_z\Lambda)$, $|\Sigma = \pm 1/2\rangle$ is the spin wave function, and Λ and Σ are the projections of the orbital and spin angular momentum onto the nuclear symmetry axis z , respectively. The wave functions $|Nn_z\Lambda\rangle$ can be further expanded into a sum of the spherical harmonic oscillator s.p. wave functions $|n_r\ell\Lambda\rangle$. Then expression (14) can be rewritten as [19,20]

$$|\tau\Omega_\tau\rangle = \sum_\chi B_\chi^\tau |\chi\Omega_\tau\rangle, \quad (15a)$$

$$|\chi\Omega_\tau\rangle = \sum_\Sigma C_{\ell\Lambda_\tau \frac{1}{2}\Sigma}^{j\Omega_\tau} |n_r\ell\Lambda_\tau = \Omega_\tau - \Sigma\rangle |\Sigma\rangle, \quad (15b)$$

$$B_\chi^\tau = \sum_{Nn_z\Sigma} C_{\ell\Lambda_\tau \frac{1}{2}\Sigma}^{j\Omega_\tau} b_{Nn_z\Sigma} A_{Nn_z\Lambda_\tau}^{n_r\ell}, \quad (15c)$$

where $\chi \equiv (n_r\ell j)$ labels the quantum numbers of the spherical harmonic oscillator wave function, $A_{Nn_z\Lambda_\tau}^{n_r\ell} = \langle n_r\ell\Lambda_\tau | Nn_z\Lambda_\tau \rangle$ is the spatial overlap integral between the spherical and the deformed harmonic oscillator wave functions, and $C_{\ell\Lambda_\tau \frac{1}{2}\Sigma}^{j\Omega_\tau}$ is the Clebsch-Gordan coefficient. Using Eq. (15), the matrix elements of T_{JK} in Eq. (13) are given by [19,20]

$$\langle p | T_{JK} | n \rangle = \sum_{\chi_p} \sum_{\chi_n} F_{p\chi_p n\chi_n}^{JK} \langle \chi_p || T_J || \chi_n \rangle / \sqrt{2J+1}, \quad (16a)$$

$$F_{p\chi_p n\chi_n}^{JK} = B_{\chi_p}^p B_{\chi_n}^n (-1)^{j_n - \Omega_n} C_{j_p \Omega_p j_n - \Omega_n}^{JK}. \quad (16b)$$

Also, the two-body deformed wave function for a proton-neutron pair characterized by K^π is given

by [19,20]

$$|p\bar{n}\rangle = \sum_{\chi_p \chi_n J} F_{p\chi_p n \chi_n}^{JK} |\chi_p \chi_n, JK\rangle, \quad (17a)$$

$$|\chi_p \chi_n, JK\rangle = \sum_{\Omega_p \Omega_n} C_{j_p \Omega_p j_n - \Omega_n}^{JK} |\chi_p \Omega_p\rangle |\chi_n - \Omega_n\rangle, \quad (17b)$$

with $\pi_p \pi_n = \pi$.

Next, we transfer our attention to the two-body interaction matrix elements $V(p\bar{n}p'\bar{n}')$ and $\tilde{V}(pn'p'n)$ in the deformed Woods-Saxon s.p. basis, which are considered to deal with the pp and ph excitations in the deformed QRPA equations. First, the two-body interaction matrix elements $G(\chi_p \chi_n \chi_{p'} \chi_{n'}, J)$ in a spherical harmonic oscillator s.p. basis are evaluated based on the Brückner G matrix with the charge-dependent Bonn nucleon-nucleon force. The details of the calculations are described in Refs. [39–41] as well as the parameters used in the calculations. Then, using Eq. (17), one can obtain [19,20]

$$V(p\bar{n}p'\bar{n}') = -2 \sum_J \sum_{\chi_p \chi_n \chi_{p'} \chi_{n'}} F_{p\chi_p n \chi_n}^{JK} F_{p'\chi_{p'} n' \chi_{n'}}^{JK} \times G(\chi_p \chi_n \chi_{p'} \chi_{n'}, J), \quad (18a)$$

$$\tilde{V}(pn'p'n) = 2 \sum_J \sum_{\chi_p \chi_{n'} \chi_{p'} \chi_n} F_{p\chi_p \bar{n}' \chi_{n'}}^{JK'} F_{p'\chi_{p'} \bar{n} \chi_n}^{JK'} \times G(\chi_p \chi_{n'} \chi_{p'} \chi_n, J), \quad (18b)$$

where $K = \Omega_p - \Omega_n = \Omega_{p'} - \Omega_{n'}$ and $K' = \Omega_p + \Omega_{n'} = \Omega_{p'} + \Omega_n$.

III. NUMERICAL RESULTS AND DISCUSSION

Before we present the numerical results for deformed neutron-rich Zr and Mo isotopes, we would like to discuss the practical aspects of our calculations. First, the s.p. energies ϵ_τ and wave functions $|\tau \Omega_\tau\rangle$ of the axially deformed Woods-Saxon potential are computed in the axially deformed harmonic oscillator basis, where the deformed Woods-Saxon potential is generated by the “universal” parametrization [38]. The heights of effective barriers for the positive-energy states are also evaluated in order to exclude spurious positive-energy solutions. In our calculations, the model space is defined by all the s.p. states with energies up to 10 MeV for protons and neutrons. This means that some quasibound states with energies $0 < \epsilon_\tau < 10$ MeV are included, in addition to negative-energy bound states. Second, the wave functions $|\tau \Omega_\tau\rangle$ are decomposed within eight major spherical harmonic oscillator shells, as shown in Eq. (15). Third, the quasiparticle energies E_τ and pairing amplitudes (v_τ, u_τ) for protons and neutrons are separately obtained by solving the BCS equations with constant pairing gaps [37,42,43]:

$$2(\epsilon_i - \lambda)u_i v_i + \Delta(v_i^2 - u_i^2) = 0, \quad (19a)$$

$$\Delta = -G \sum_i u_i v_i, \quad E_i = \sqrt{(\epsilon_i - \lambda)^2 + \Delta^2}. \quad (19b)$$

The empirical pairing gaps Δ_τ are extracted from the nucleon separation energies [44]. They are taken either from the

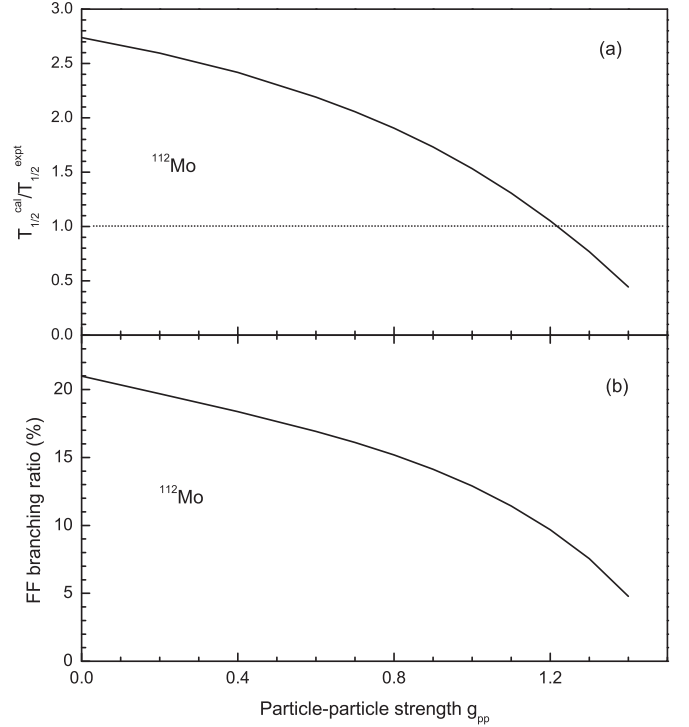


FIG. 1. Dependence of the calculated β^- decay rates on the g_{pp} value for the β^- decay of ^{112}Mo : (a) ratio of the calculated half-life to the experimental data versus particle-particle strength g_{pp} , (b) branching ratio for FF transitions versus particle-particle strength g_{pp} .

AME2012 atomic mass evaluation, when available [44], or from the KUTY mass formula [45].

Finally, the different intrinsic excitations are considered for β transitions using the QRPA matrix equations. The response function of GT transitions contains three components, $K^\pi = 0^+, \pm 1^+$, and the response function of FF transitions contains five components, $K^\pi = 0^-, \pm 1^-, \pm 2^-$. In expressions (11) and (12) of submatrices A and B , the ph and pp interaction elements are renormalized by the strength parameters g_{ph} and g_{pp} . Here, we use the same g_{ph} and g_{pp} for all components K^π . This makes the calculation straightforward and maintains the relative strength of different components. It is known that the ph channel mainly determines the energy position of GT giant resonances (GTGRs) at a high excitation energy [46], which is observed by (p, n) charge-exchange reactions. As there is no available information on the GTGR energy for the nuclei under investigation, the g_{ph} strength is adjusted to reproduce the empirical GTGR energy [46]. It has a value of approximately $g_{ph} = 1.00$. Unfortunately, one cannot obtain explicit information on the g_{pp} strength from (p, n) reactions like the g_{ph} strength. The feasible way is to use the experimental β^- -decay half-lives to fix the g_{pp} strength. We now discuss the sensitivity of the calculated β -decay properties to the g_{pp} strength. For concreteness, we take the β^- decay of ^{112}Mo as an example. All other β emitters show similar sensitivities. Figure 1(a) shows the ratio of the calculated half-life to the experimental data as a function of the g_{pp} value for the β^- decay of ^{112}Mo , where the quenching is taken

TABLE I. Spin parities, excitation energies, and $\log ft$ values of several important decay branches for the GT and FF transitions of ^{112}Mo . These decay branches make a relatively large contribution to the decay width. Calculations are separately performed with $g_{pp} = 0.0, 0.8, \text{ and } 1.2$. The unit of the excitation energies is MeV.

	$g_{pp} = 0.0$			$g_{pp} = 0.8$			$g_{pp} = 1.2$		
	K^π	E_{ex}	$\log ft$	K^π	E_{ex}	$\log ft$	K^π	E_{ex}	$\log ft$
GT	1^+	1.238	5.86	0^+	0.354	5.99	0^+	0.159	4.87
	1^+	1.502	5.11	0^+	1.268	4.64	0^+	0.383	5.49
	1^+	1.635	4.55	1^+	1.289	5.35	0^+	0.957	4.43
	0^+	1.694	5.67	1^+	1.396	4.78	1^+	1.180	4.83
	0^+	1.709	5.74	0^+	1.464	5.51	0^+	1.313	5.33
	1^+	2.330	5.39	1^+	2.068	5.24	1^+	1.718	5.19
FF	0^-	0.482	6.18	0^-	0.321	5.82	0^-	0.010	5.93
	0^-	0.763	5.56	0^-	0.410	6.29	1^-	0.031	6.83
	0^-	1.116	6.13	0^-	0.720	5.83	1^-	0.733	6.60
	1^-	1.109	6.36	1^-	1.003	6.07	1^-	0.875	6.07
	1^-	1.172	6.19	0^-	1.996	6.11	0^-	1.735	6.35
	0^-	2.311	6.09	0^-	2.026	6.22	0^-	1.841	6.01
	0^-	2.633	5.88	0^-	2.581	5.71	0^-	2.523	5.80

into account using $(g_A/g_V)_{\text{eff}} = 0.77(g_A/g_V)_{\text{free}}$ [16]. If the g_{pp} value is varied from 0.4 to 1.2, the half-life decreases by more than 50%. This effect can be easily understood in terms of the general Sargent law $T_{1/2} \propto 1/(Q_\beta - E_f)^5$ or the new exponential law for β -decay half-lives [47,48], because increasing the pp interaction would cause a lowering of the excitation energies E_f [49]. Here, we adopt a g_{pp} strength of $g_{pp} = 1.10$ for all nuclei under investigation.

One important aspect of the present calculation is that both GT and FF transitions are taken into account to calculate β -decay rates. This provides a good opportunity to investigate the contribution of FF transitions to half-lives. It is found that the contribution of FF transitions is correlated with the g_{pp} strength as well. Figure 1(b) illustrates the branching ratio for FF transitions as a function of the g_{pp} value for the β^- decay of ^{112}Mo . As the g_{pp} value is increased from 0.4 to 1.2, the calculated branching ratio for FF transitions is decreased from 18% to 9%. To be specific, the decay width of GT transitions is increased by a factor of roughly 2.6, while the decay width of FF transitions is increased by a factor of about 1.2. Obviously, the effect of the g_{pp} strength is more considerable on GT transitions than on FF transitions. Nowadays there is rare information on the contribution of FF transitions in experiments. The correlation between the g_{pp} strength and the competition of GT and FF transitions is worth further investigations from both the experimental and the theoretical sides. Moreover, in order to gain insight into the effect of the g_{pp} strength on the nuclear matrix element, we also list in Table I the spin parities K^π , excitation energies E_{ex} , and $\log ft$ values for some important GT and FF transitions in the β^- decay of ^{112}Mo . These transitions make a relatively large contribution to the decay width. Note that calculations are separately performed with different g_{pp} strengths, $g_{pp} = 0.0, 0.8, \text{ and } 1.2$.

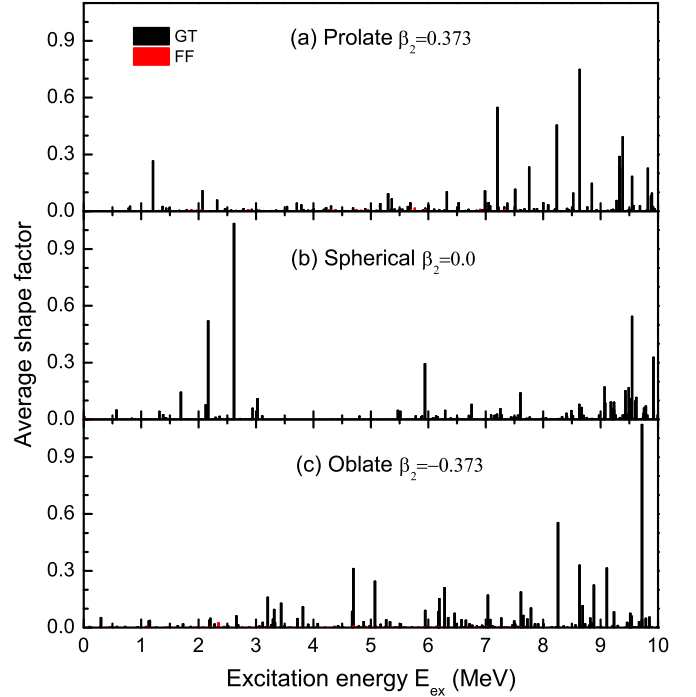


FIG. 2. (Color online) Low-lying average shape factors for GT and FF transitions as a function of the excitation energy E_{ex} for the β^- decay of ^{106}Zr . (a) Average shape factors for GT and FF transitions calculated in the prolate shape with $\beta_2 = 0.373$, which is suggested by the FRDM in Ref. [3]; (b) results calculated in the spherical shape with $\beta_2 = 0.0$; (c) results calculated in the oblate shape with $\beta_2 = -0.373$. The shape factor for GT transitions is denoted by black lines and the average shape factor for FF transitions is denoted by lighter (red) lines.

To illustrate the strength of FF transitions, one usually employs the average shape factor $\overline{C(W)}$ instead of the shape factor $C(W)$, since the shape factor $C(W)$ of FF transitions depends on the β energy W as shown in Eq. (4). The average shape factor is defined as [24]

$$\overline{C(W)} = f(Z, R, W_0)/f_0(Z, R, W_0), \quad (20)$$

where $f(Z, R, W_0)$ is defined in Eq. (1) and $f_0(Z, R, W_0)$ is given by

$$f_0(Z, R, W_0) = \int_1^{W_0} dW F(Z, R, W)(W_0 - W)^2 \times W \sqrt{W^2 - 1}. \quad (21)$$

We show the low-lying average shape factors for the β^- decay of ^{106}Zr as an example. In order to discern the effect of nuclear deformations, prolate, spherical, and oblate shapes are considered. Figure 2 illustrates the average shape factors for GT and FF transitions as a function of the excitation energy E_{ex} . It is clearly shown that the deformation leads to fragmentation of the dominant peak into several weaker peaks and transfer of part of the strength from the lower excitation energy region to the higher excitation energy region. Moreover, the peaks shown in Fig. 2(a)–2(c) are located at various positions. Consequently, calculations with the different

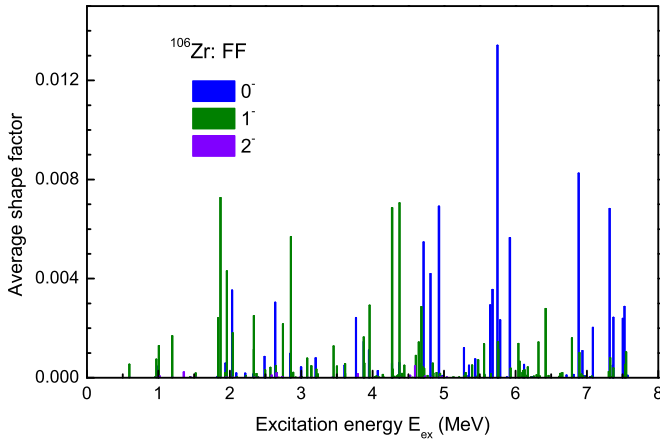


FIG. 3. (Color online) Low-lying average shape factors for different components 0^- , 1^- , and 2^- of FF transitions as a function of the excitation energy E_{ex} for the β^- decay of ^{106}Zr . Calculations are performed in the prolate shape with $\beta_2 = 0.373$, which is suggested by the FRDM in Ref. [3].

shapes yield different half-lives: $T_{1/2} = 246$ ms for the prolate shape, $T_{1/2} = 105$ ms for the spherical shape, and $T_{1/2} = 148$ ms for the oblate shape. The tendency of the calculated half-life with the nuclear shape is consistent with the results in Ref. [16]. To gain more insight into the average shape factor for FF transitions, we display in Fig. 3 the average shape factor within the Q_β window, which is calculated with the prolate shape suggested by the FRDM [3]. As shown in Fig. 3, the average shape factor is divided into three components, which separately

correspond to 0^- , 1^- , and 2^- transitions. One can see that the components of 0^- and 1^- transitions significantly contribute to FF transitions. The component of 1^- transitions is preferred in the lower energy region, while the component of 0^- transitions takes a dominant place in the higher energy region. It should be particularly noted that the average shape factor with the lower excitation energy makes more of a contribution to the decay width, owing to larger f_0 values. As a consequence, the contribution of 1^- transitions is dominant and the next one is that of 0^- transitions, even though the component of 0^- transitions is relatively larger than that of 1^- transitions.

Using the formalism described above, we have performed a detailed calculation of the β^- -decay half-lives of even-even Zr and Mo isotopes. In our calculations, the set of deformation parameters ($\beta_2, \beta_4, \beta_6$) is taken from the results of Möller *et al.* [3] unless otherwise stated. The experimental β -decay half-lives are taken from Ref. [50], and some new data obtained with improved accuracy or measured for the first time are taken from Ref. [12]. In Fig. 4, we present a comparison of the present results with the available data for the neutron-rich Zr and Mo isotopes. For comparison, the theoretical results of Möller *et al.* are also shown, where GT transitions are considered within the FRDM plus QRPA using ph terms of separable residual interactions and FF transitions are taken into account by the gross theory [10]. Circles, squares, and triangles represent the available experimental data, the results of this work, and the results in Ref. [10], respectively. Three regions are distinguished in Fig. 4, according to the source of Q_β values: region I, where experimental Q_β values [44] are used; region II, where Q_β values obtained from systematics [44] are used; and region III, where theoretical Q_β values obtained

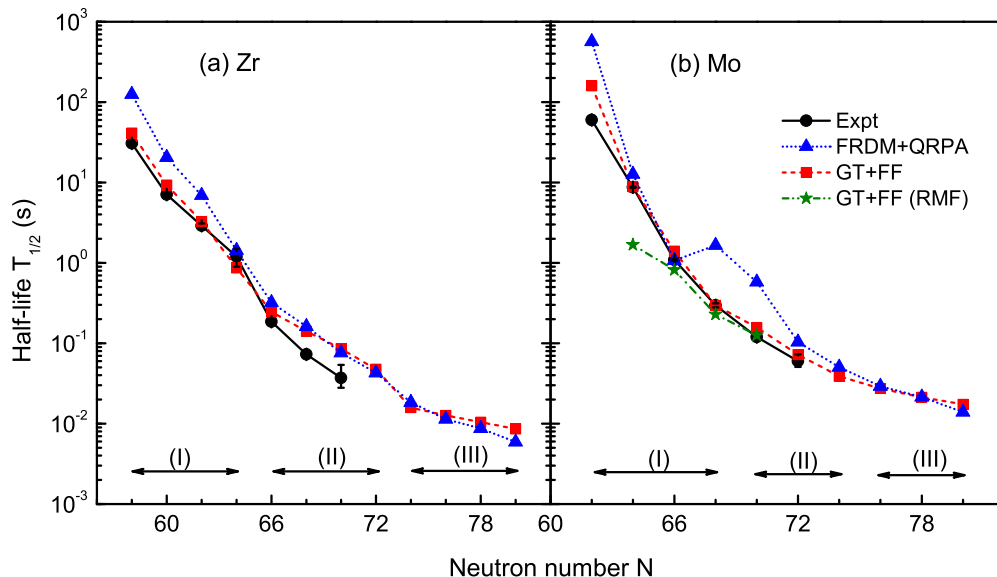


FIG. 4. (Color online) Comparison of the calculated half-lives [denoted GT + FF] with the available experimental data (labeled Expt) for neutron-rich Zr and Mo isotopes. The theoretical results of Möller *et al.* (denoted FRDM + QRPA) are also shown for comparison [10], including the calculations for both GT and FF transitions. For $^{106-112}\text{Mo}$, calculations are also performed with the deformation parameters predicted by the RMF [5], where negative values for the quadrupole deformation parameter β_2 are suggested, in contrast to the FRDM predictions, and the corresponding results [denoted GT + FF (RMF)] are displayed in (b). Three regions (I–III) are distinguished, according to the source of the Q_β values used in the calculations: (I) experimental Q_β values [44], (II) Q_β values obtained from systematics [44], and (III) theoretical Q_β values obtained from the KUTY mass formula [45].

from the KUTY mass formula [45] are used. The uncertainty of experimental Q_β values is about 10 keV in region I, while the uncertainty of Q_β values is more than 200 keV in region II. Specifically, the experimental Q_β value for ^{104}Zr (in region I) is known to be 6095(10) keV. The uncertainty of 10 keV brings in an uncertainty in the calculated half-life of ± 8 ms, corresponding to an effect of about $\pm 0.9\%$. For ^{112}Mo (in region II), the uncertainty of $Q_\beta = 7790(200)$ keV leads to an uncertainty in the calculated half-life of $-21/+25$ ms, corresponding to an effect of roughly $-13.4/+15.8\%$.

In Fig. 4(a), the FRDM + QRPA calculations generally overestimate the experimental half-lives to some extent. The reason for this may be that the pp interaction is not included in the QRPA calculation [10], resulting in an overestimation of the excitation energy of the daughter states. By contrast, the present calculations yield shorter half-lives and show a good agreement with the experimental data. For $^{108,110}\text{Zr}$, there are slightly large deviations from the experimental data, by a factor of about 2. This may be attributed to the large uncertainties in the Q_β values, as mentioned above. One can also note that there is a strong decrease in the experimental half-life at the neutron number across $N = 64$, which gives an active response to the deformed subshell closure $N = 64$. The present calculations reproduce this feature well. For $^{106-112}\text{Mo}$, the FRDM suggests positive values for the quadrupole deformation parameter β_2 [3], while the RMF yields negative values [5]. With this in mind, we also evaluate the half-lives of $^{106-112}\text{Mo}$ using the deformation parameters predicted by RMF calculations, which are represented as stars in Fig. 4(b). One can see that the half-lives calculated with the FRDM deformation parameters are always larger than those calculated with the RMF deformation parameters and the discrepancy between them becomes smaller with increasing neutron number. This agrees well with the results in Ref. [16]. The standard deviation of the calculated β -decay half-lives for 13 nuclei is obtained as $\sigma = \{ \sum_{i=1}^{13} [\log_{10}(T_{\text{expt}}^i / T_{\text{calc}}^i)]^2 / 12 \}^{1/2} = 0.20$, which corresponds to a factor of less than 1.60. As additional information, the standard deviation of the FRDM + QRPA results is evaluated as well, $\sigma = 0.51$ corresponding to a factor of about 3.21. In addition, the present calculations are extended to some other neutron-rich isotopes, including $^{112-120}\text{Zr}$ and $^{116-122}\text{Mo}$. As one would expect, the calculated half-lives

show a decreasing trend with increasing neutron number. More importantly, the discrepancy between the FRDM + QRPA results and the present calculations becomes smaller with increasing neutron number. This demonstrates a good convergence of the theoretical predictions.

IV. SUMMARY

In summary, we have presented in this paper the deformed QRPA with realistic nucleon-nucleon interactions to calculate the β -decay half-lives of neutron-rich Zr and Mo isotopes. Within the deformed QRPA, the deformed s.p. basis is computed by solving the Schrödinger equation with the axially deformed Woods-Saxon potential, and the residual particle-particle and particle-hole interaction matrix elements in the deformed s.p. basis are obtained in terms of the Brückner G matrix with the charge-dependent Bonn nucleon-nucleon force. The contributions from allowed GT and FF transitions are considered using the different response functions. The sensitivity of the calculated β -decay properties to the particle-particle strength is discussed, and the parameters used in the calculations are explained in detail. The calculated results shown in Fig. 4 are in good agreement with the available experimental data and consistent with the theoretical results of FRDM + QRPA. Moreover, predictions of β -decay half-lives are made for more neutron-rich Zr and Mo isotopes, which could be useful for future experiments.

ACKNOWLEDGMENTS

This work is supported by the National Natural Science Foundation of China (Grant Nos. 10735010, 10975072, 11035001, 11120101005, and 11375086), by 973 National Major State Basic Research and Development of China (Grant Nos. 2013CB834400 and 2010CB327803), by a Project Funded by the Priority Academic Programme Development of JiangSu Higher Education Institutions (PAPD), by the Research Fund of Doctoral Point (RFDP; Grant No. 20100091110028), by the Science and Technology Development Fund of Macau (Grant No. 068/2011/A), and by a China Postdoctoral Science Foundation-funded project (Grant No. 2013M530246).

-
- [1] J. K. Hwang, A. V. Ramayya, J. H. Hamilton, Y. X. Luo, A. V. Daniel, G. M. Ter-Akopian, J. D. Cole, and S. J. Zhu, *Phys. Rev. C* **73**, 044316 (2006).
- [2] T. Sumikama, K. Yoshinaga, H. Watanabe *et al.*, *Phys. Rev. Lett.* **106**, 202501 (2011).
- [3] P. Möller, J. R. Nix, W. D. Myers, and W. J. Swiatecki, *At. Data Nucl. Data Tables* **59**, 185 (1995).
- [4] J. Skalski, S. Mizutori, and W. Nazarewicz, *Nucl. Phys. A* **617**, 282 (1997).
- [5] G. A. Lalazissis, S. Raman, and P. Ring, *At. Data Nucl. Data Tables* **71**, 1 (1999).
- [6] S. Goriely, F. Tondeur, and J. M. Pearson, *At. Data Nucl. Data Tables* **77**, 311 (2001).
- [7] S. Goriely, M. Samyn, P.-H. Heenen, J. M. Pearson, and F. Tondeur, *Phys. Rev. C* **66**, 024326 (2002).
- [8] J. J. Cowan, F. K. Thielemann, and J. W. Truran, *Phys. Rep.* **208**, 267 (1991).
- [9] K. L. Kratz, J. P. Bitouzet, F. K. Thielemann, P. Möller, and B. Pfeiffer, *Astrophys. J.* **403**, 216 (1993).
- [10] P. Möller, B. Pfeiffer, and K. L. Kratz, *Phys. Rev. C* **67**, 055802 (2003).
- [11] J. Pereira, S. Henrich, A. Aprahamian *et al.*, *Phys. Rev. C* **79**, 035806 (2009).
- [12] S. Nishimura, Z. Li, H. Watanabe *et al.*, *Phys. Rev. Lett.* **106**, 052502 (2011).

- [13] P. Sarriguren, E. Moya de Guerra, L. Paceaescu, Amand Faessler, F. Šimkovic, and A. A. Raduta, *Phys. Rev. C* **67**, 044313 (2003).
- [14] F. Šimkovic, L. Paceaescu, and A. Faessler, *Nucl. Phys. A* **733**, 321 (2004).
- [15] H. Homma, E. Bender, M. Hirsch, K. Muto, H. V. Klapdor-Kleingrothaus, and T. Oda, *Phys. Rev. C* **54**, 2972 (1996).
- [16] P. Sarriguren and J. Pereira, *Phys. Rev. C* **81**, 064314 (2010); P. Sarriguren, A. Algora, and J. Pereira, *ibid.* **89**, 034311 (2014).
- [17] P. Sarriguren, E. Moya de Guerra, A. Escuderos, and A. C. Carrizo, *Nucl. Phys. A* **635**, 55 (1998).
- [18] M. Martini, S. Péru, and S. Goriely, *Phys. Rev. C* **89**, 044306 (2014).
- [19] M. S. Yousef, V. Rodin, A. Faessler, and F. Šimkovic, *Phys. Rev. C* **79**, 014314 (2009).
- [20] D.-L. Fang, A. Faessler, V. Rodin, and F. Šimkovic, *Phys. Rev. C* **83**, 034320 (2011).
- [21] D.-L. Fang, B. A. Brown, and T. Suzuki, *Phys. Rev. C* **88**, 024314 (2013).
- [22] D. Ni and Z. Ren, *J. Phys. G: Nucl. Part. Phys.* **41**, 025107 (2014).
- [23] T. Suzuki, T. Yoshida, T. Kajino, and T. Otsuka, *Phys. Rev. C* **85**, 015802 (2012).
- [24] Q. Zhi, E. Caurier, J. J. Cuenca-García, K. Langanke, G. Martínez-Pinedo, and K. Sieja, *Phys. Rev. C* **87**, 025803 (2013).
- [25] H. Behrens and W. Bühring, *Electron Radial Wave Functions and Nuclear Beta-Decay* (Clarendon, Oxford, UK, 1982).
- [26] H. Behrens and W. Bühring, *Nucl. Phys. A* **162**, 111 (1971).
- [27] P. Vogel and M. R. Zirnbauer, *Phys. Rev. Lett.* **57**, 3148 (1986); J. Engel, P. Vogel, and M. R. Zirnbauer, *Phys. Rev. C* **37**, 731 (1988).
- [28] K. Muto, E. Bender, T. Oda, and H. V. Klapdor-Kleingrothaus, *Z. Phys. A* **341**, 407 (1992).
- [29] J. Suhonen and O. Civitarese, *Phys. Lett. B* **280**, 191 (1992).
- [30] M. K. Cheoun, A. Bobyk, A. Faessler, F. Šimkovic, and G. Teneva, *Nucl. Phys. A* **561**, 74 (1993).
- [31] J. Engel, M. Bender, J. Dobaczewski, W. Nazarewicz, and R. Surman, *Phys. Rev. C* **60**, 014302 (1999).
- [32] D. Ni and Z. Ren, *J. Phys. G: Nucl. Part. Phys.* **39**, 125105 (2012).
- [33] D. Ni, Z. Ren, and Q. Zhi, *Sci. China-Phys. Mech. Astron.* **55**, 2397 (2012).
- [34] H. Li and Z. Ren, *Sci. China-Phys. Mech. Astron.* **57**, 1005 (2014).
- [35] D. J. Millener, D. E. Alburger, E. K. Warburton, and D. H. Wilkinson, *Phys. Rev. C* **26**, 1167 (1982).
- [36] A. Bohr and B. R. Mottelson, *Nuclear Structure, Vol. II: Nuclear Deformations* (World Scientific, Singapore, 1998).
- [37] P. Ring and P. Schuck, *The Nuclear Many-Body Problem* (Springer-Verlag, Berlin, 1980).
- [38] S. Cwiok, J. Dudek, W. Nazarewicz, J. Skalski, and T. Werner, *Comput. Phys. Commun.* **46**, 379 (1987).
- [39] H. M. Sommermann, H. Müther, K. C. Tam, T. T. S. Kuo, and A. Faessler, *Phys. Rev. C* **23**, 1765 (1981).
- [40] M. Hjorth-Jensen, T. T. S. Kuo, and E. Osnes, *Phys. Rep.* **261**, 125 (1995).
- [41] D. J. Dean, T. Engeland, M. Hjorth-Jensen, M. P. Kartamyshev, and E. Osnes, *Prog. Part. Nucl. Phys.* **53**, 419 (2004).
- [42] M. Rho and J. O. Rasmussen, *Phys. Rev.* **135**, B1295 (1964).
- [43] Z. Ren, Z. Y. Zhu, Y. H. Cai, and G. Xu, *Phys. Lett. B* **380**, 241 (1996).
- [44] M. Wang, G. Audi, A. H. Wapstra, F. G. Kondev, M. MacCormick, X. Xu, and B. Pfeiffer, *Chinese Phys. C* **36**, 1603 (2012).
- [45] H. Koura, T. Tachibana, M. Uno, and M. Yamada, *Prog. Theor. Phys.* **113**, 305 (2005).
- [46] J. Suhonen, T. Taigel, and A. d. Faessler, *Nucl. Phys. A* **486**, 91 (1988).
- [47] X. Zhang and Z. Ren, *Phys. Rev. C* **73**, 014305 (2006).
- [48] Y. Ren and Z. Ren, *Phys. Rev. C* **89**, 064603 (2014).
- [49] J. Suhonen, *From Nucleons to Nucleus: Concepts of Microscopic Nuclear Theory* (Springer, Berlin, 2007).
- [50] NNDC of the Brookhaven National Laboratory; <http://www.nndc.bnl.gov/>.